J|A|C|S ARTICLES

Published on Web 01/27/2009

Zinc Oxide Nanostructures Confined in Porous Silicas

Benoit Coasne,*,† Aude Mezy,† R. J. M. Pellenq,‡ D. Ravot,† and J. C. Tedenac†

Institut Charles Gerhardt Montpellier, UMR 5253 CNRS, Université Montpellier 2, ENSCM, Place Eugène Bataillon, 34095 Montpellier Cedex 05, France, Department of Civil and Environmental Engineering, Massachusetts Institute of Technology, 77, Massachusetts Avenue, Cambridge, Massachusetts 02139, and Centre Interdisciplinaire des Nanosciences de Marseille, UPR 3118 CNRS, Campus de Luminy, 13288 Marseilles, France

Received August 22, 2008; E-mail: benoit.coasne@univ-montp2.fr

Abstract: We report on molecular simulations of zinc oxide nanostructures obtained within silica nanopores of diameter $D = 1.6$ nm and $D = 3.2$ nm. Both the effects of confinement (by varying the pore size) and degree of pore filling on the structure of the nanomaterial are addressed. Two complementary approaches are adopted: 1) the stability of the three crystalline phases of ZnO (wurtzite, rocksalt, and blende) in the silica nanopores is studied, and 2) ZnO nanostructures are obtained by slowly cooling down a homogeneous liquid phase confined in the silica pores. None of the ideal nanostructures (wurtzite, rocksalt, blende) retains the ideal structure of the initial crystal when confined within the silica pores. Only the structure starting from the ideal wurtzite nanocrystal remains significantly crystalline after relaxation, as revealed by the marked peaks in the pair correlation functions for this system. The morphology and degree of cristallinity of the structures are found to depend on the parameters involved in the synthesis (pore size, filling density). Nanograin boundaries are observed between domains of different crystal structures. Reminiscent features of the bulk behavior, such as faceting of the nanostructures, are also observed when the system size becomes large. We show that the use of nanopores as a template imposes that the confined particles exhibit neutral (basal) surfaces. These predictions provide a guide to experiments on semiconductor nanoparticles.

1. Introduction

Owing to their unique optical and electronical properties, semiconductors, nanowires, or nanotubes are of crucial interest for new technologies. These nanostructures are a key element for the development of nanoscale applications for microelectronics (ultrascaled microprocessors), chemical and biological sensing, and energy conversion storage (solar cells, batteries).[1−3] Among possible semiconductors to be brought to the nanoscale, zinc oxide (ZnO) is a desirable candidate as it is a semiconductor with a direct wide band gap of 3.37 eV at room temperature and a large exciton energy of 60 meV.[4] An exhaustive review of the work done on ZnO nanostructures is a tedious task which is out of the scope of the present paper (as noted by Klingshirn in ref 5, more than 2000 ZnO-related articles were published in 2005 and many of them deal with ZnO nanostructures). Excellent reviews have been recently published on the synthesis of ZnO nanoobjects and their use[5−8] for fundamental and applied research. From an experimental point of view, many methods have been employed for the growth of ZnO nanomaterials, such as radiofrequency magnetron sputtering, chemical vapor deposition, spray pyrolysis, thermal evaporation, electrophoretic deposition, etc.[9−14] Nanoporous materials used as a template also provide a simple way to obtain ZnO nanostructures. As a result, many porous materials have been used to prepare ZnO nanostructures: zeolites,[15,16] porous silicon,[17] porous alumina,[18,19] porous carbons,[20] porous silicas[21−29] (micelle-templated porous materials). Among these nanoporous solids, the siliceous MCM-41[30] and SBA-15[31] are important materials because they exhibit pores of a simple geometry and uniform size. These materials are obtained by a templating

† Université Montpellier 2.

‡ Massachusetts Institute of Technology and Centre Interdisciplinaire des Nanosciences de Marseille.

(1) Chau, R.; Doyle, B.; Datta, S.; Kavalieros, J.; Zhang, K. *Nat. Mater.* **2007**, *6*, 810.
(2) Qin, Y.; Wang, X.; Wang, Z. L. *Nature* **2008**, *451*, 809.
(3) Klauk, H. *Nature* **2008**, *451*, 533.
(4) Tian, Z. R.; Voigt, J. A.; Liu, J.; McKenzie, B.; McDermott, M. J.; Rodriguez, M. A.; Konishi, H.; Xu, H. *Nat. Mater.* **2003**, *2*, 821.
(5) Klingshirn, C. *Chem. Phys. Chem.* **2007**, *8*, 782.
(6) Djurisic, A. B.; Leung, Y. H. *Small* **2006)** , *2*, 944.
(7) Wang, Z. L. *Mater. Today* **2007**, *10*, 20.
(8) Schmidt-Mende, L.; MacManus-Driscoll, J. L. *Mater. Today* **2007**, *10*, 40.
(9) Matsumoto, K.; Konemura, K.; Shimaoka, G. *J. Cryst. Growth* **1985**, *71*, 1.
(10) Ishikawa, Y.; Shimizu, Y.; Sasaki, T.; Koshizaki, N. *J. Colloid Interface Sci.* **2006**, *300*, 2.
(11) Zhao, J.; Jin, Z. G.; Li, T.; Liu, X. X. *Appl. Surf. Sci.* **2006**, *252*, 23.
(12) Krunks, M.; Dedova, T.; Oja Acik, I. *Thin Solid Films* **2006**, *515*, 1157.
(13) Boccaccini, A. R.; Roether, J. A.; Thomas, B. J. C.; Shaffer, M. S. P.; Chavez, E.; Stoll, E.; Minay, E. J. *J. Ceram. Soc. Jpn.* **2006**, *114*, 1.
(14) Hu, Y.; Chen, J. F. *J. Cluster Sci.* **2007**, *18*, 371.
(15) Tkachenko, O. P.; Klementiev, K. V.; Loffler, E.; Ritzkopf, I.; Schuth, F.; Bandyopadhyay, M.; Grabowski, S.; Gies, H.; Hagen, V.; Muhler, M.; Lu, L.; Fischere, R. A.; Grunert, W. *Phys. Chem. Chem. Phys.* **2003**, *5*, 4325.
(16) Bouvy, C.; Marine, W.; Sporken, R.; Su, B. L. *Colloid Surf. A* **2007**, *300*, 145.
(17) Singh, R. G.; Singh, F.; Agarwal, V.; Mehra, R. M. *J. Phys. D: Appl. Phys.* **2007**, *40*, 3090.

mechanism involving formation of surfactant or block copolymer micelles in a mixture composed of a solvent and a silica source. After polymerization of the silica and removal of the organic micelles one obtains a material made up of an array of regular pores. The pore diameter distribution is narrow with an average value that can be varied from 2 to 20 nm depending on the synthesis conditions. From a fundamental point of view, MCM-41 and SBA-15 are considered as model materials to investigate the effect of nanoconfinement on the thermodynamic properties of fluids. In particular, the cylindrical geometry of the pores in these materials makes it possible to address in a simple way the effect of confinement on the adsorption, capillary condensation, and freezing/melting of fluids in nanopores. As a result, many experimental, theoretical, and molecular simulation studies have been reported on the thermodynamics of fluids confined in these materials (for reviews, see refs 32 and 33).

Of particular interest for the present work, some authors clearly demonstrate formation of ZnO within the pores of the host material. For instance, Seo et al. showed that ZnO nanotubes obtained within porous alumina have regular morphologies and well-defined diameters after selective etching of the initial porous material.[19] Using solid-state nuclear magnetic reasonance and Fourier transform infrared spectroscopy, Schroder et al. also demonstrated formation of ZnO within MCM-48 by the disappearance of Si−OH groups at the surface of the porous material.[26] From a liquid precursor, Polarz et al.[34] obtained monodispersed ZnO nanoclusters in the pores of a MCM-48-like silica porous material. It is shown that confinement determines the hierarchical architecture of the final ZnO/SiO_2 nanocomposites. Molecular modeling of ZnO nanostructures confined in nanopores has received considerably less attention. Jentys and Grimes[35] studied ZnO structures embedded in a nanoporous material. Using molecular simulation, these authors showed that small ZnO clusters confined in zeolite (Faujasite) present significant distortions that cause energy penalties. More recently, Kulkarni et al.[36,37] and Tu and Xu[38] used molecular dynamics and first-principles calculations to study the stability of ZnO nanoobjects and found evidence for a novel phase transformation in ZnO nanowires from wurtzite to a graphite-like hexagonal structure. Such a new surface-driven phase transition (for a recent review on confinement effect on crystallization, see also ref 33) might occur in confined systems and are, thus, relevant for studies on materials embedded in porous matrices. Besides specific works on formation of ZnO nanostructures, studies of confined molten salt or ionic crystals have been reported.[39−42] Using high-resolution transmission electronic microscopy, Meyer et al.[39] have shown that the freezing of potassium iodide confined in a 1.6 nm single-wall carbon nanotube occurs at a temperature significantly larger than the bulk freezing point. Moreover, the lattice spacing of the confined solid was found to be different than that of the bulk crystal.[39] Wilson compared the experimental data by Meyer et al.[39] with molecular simulations for confined potassium iodide and found that the radius of the carbon nanotube has a crucial effect on formation of the confined crystal.[40]

The present work reports a molecular simulation study of ZnO nanostructures confined within cylindrical silica nanopores (MCM-41). The simulations of the ZnO nanomaterial embedded in the porous matrix were carried out using the Monte Carlo algorithm in the canonical ensemble. We also report some additional molecular dynamics simulations and free-energy calculations to further test and characterize the stability of the nanoparticles. We address both the effect of confinement (by varying the pore size) and that of the filling density of the pores on the dimensionality and crystallinity of the confined material. The structure of the confined material is analyzed using pair correlation functions, which are compared with those obtained for ideal ZnO crystal structures (wurtzite, rocksalt, and blende). The crystalline order of the nanoparticles is also investigated using geometrical order parameters such as the angle between nearest neighbors. The effect of removing the host silica solid is also discussed. We show that the resulting nanosystems exhibit significant structural defects compared to the bulk; for instance, nanograin boundaries are observed between domains of different crystal structures. Reminiscent features of the bulk behavior, such as faceting of the nanostructure, are also observed when the system size becomes large. The remainder of the paper is organized as follows. In section 2 we briefly discuss the details of the simulation techniques. Section 3 presents the results obtained from the atomistic simulations of ZnO in our numerical model of silica pore MCM-41 (described as a single cylindrical silica nanopore). Section 4 contains concluding remarks and suggestions for future work.

(18) Chen, W.; Tao, X.; Liu, Y.; Sun, X.; Hu, Z.; Fei, B. *Appl. Surf. Sci.* **2006**, *252*, 8683.
(19) Seo, B. I.; Shaislamov, U. A.; Ha, M. H.; Kim, S. W.; Kim, H. K. *Physica E* **2007**, *37*, 241.
(20) Wagner, T.; Waitz, T.; Roggenbuck, J.; Froba, M.; Kohl, C. D.; Tiemann, M. *Thin Solid Films* **2007**, *515*, 8360.
(21) Shi, J. Y.; Chen, J.; Feng, Z. C.; Wang, X. L.; Ying, P. L.; Li, C. *J. Phys Chem. B* **2006**, *110*, 25612.
(22) Dapurkar, S. E.; Badamali, S. K.; Selvam, P. *Catal. Today* **2001**, *68*, 63.
(23) Tang, G. Q.; Xiong, Y.; Zhang, L. Z.; Zhang, G. L. *Chem. Phys. Lett.* **2004**, *395*, 97.
(24) Xiong, Y.; Zhang, L. Z.; Tang, G. Q.; Zhang, G. L.; Chen, W. J. *J. Lumin.* **2004**, *110*, 17.
(25) Chen, H. G.; Shi, J. L.; Chen, H. R.; Yan, J. N.; Li, Y. S.; Hua, Z. L.; Yang, Y.; Yan, D. S. *Opt. Mater.* **2004**, *25*, 79.
(26) Schroder, F.; Hermes, S.; Parala, H.; Hikov, T.; Muhler, M.; Fischer, R. *J. Mater. Chem.* **2006**, *16*, 3565.
(27) Burova, L. I.; Petukhov, D. I.; Eliseev, A. A.; Lukashin, A. V.; Tretyakov, Y. D. *Superlattices Microstruct.* **2006**, *39*, 257.
(28) Jiang, Q.; Wu, Z. Y.; Wang, Y. M.; Cao, Y.; Zhou, C. F.; Zhu, J. H. *J. Mater. Chem.* **2006**, *16*, 1536.
(29) Zeng, W.; Wang, Z.; Qian, X. F.; Yin, J.; Zhu, Z. K. *Mater. Res. Bull.* **2006**, *41*, 1155.
(30) Beck, J. S.; Vartulli, J. C.; Roth, W. J.; Leonowicz, M. E.; Kresge, C. T.; Schmitt, K. D.; Chu, C. T.-W.; Olson, D. H.; Sheppard, E. W.; McCullen, S. B.; Higgins, J. B.; Schlenker, J. L. *J. Am. Chem. Soc.* **1992**, *114*, 10834.
(31) Zhao, D.; Feng, J.; Huo, Q.; Melosh, N.; Fredrickson, G. H.; Chmelka, B. F.; Stucky, G. D. *Science* **1998**, *279*, 548.
(32) Gelb, L. D.; Gubbins, K. E.; Radhakrishnan, R.; Sliwinska-Bartkowiak, M. *Rep. Prog. Phys.* **1999**, *62*, 1573.
(33) Alba-Simionesco, C.; Coasne, B.; Dosseh, G.; Dudziak, G.; Gubbins, K. E.; Radhakrishnan, R.; Sliwinska-Bartkowiak, M. *J. Phys.: Condens. Matter* **2006**, *18*, R15.
(34) Polarz, S.; Neues, F.; van den Berg, M. W. E.; Grunert, W.; Khodeir, L. *J. Am. Chem. Soc.,* **2005**, *127*, 12028.
(35) Jentys, A.; Grimes, R. W. *J. Chem. Soc., Faraday Trans.* **1996**, *92*, 2093.
(36) Kulkarni, A. J.; Zhou, M.; Ke, F. *J. Nanotechnol.* **2005**, *16*, 2749.
(37) Kulkarni, A. J.; Zhou, M.; Sarasamak, K.; Limpijumnong, S. *Phys. Rev. Lett.* **2006**, *97*, 105502.
(38) Tu, Z. C.; Hu, X. *Phys. Rev. B* **2006**, *74*, 035434.
(39) Meyer, R. R.; Sloan, J.; Dunin-Borkowski, R. E.; Kirkland, A. I.; Novotny, M. C.; Bailey, S. R.; Hutchinson, J. L.; Green, L. M. H. *Science* **2000**, *289*, 1324.
(40) Wilson, M.; Madden, P. A. *J. Am. Chem. Soc.* **2001**, *123*, 2101.
(41) Wilson, M. *J. Chem. Phys.* **2002**, *116*, 3027.
(42) Bichoutskaia, E.; Pyper, N. C. *J. Chem. Phys.* **2008**, *129*, 154701.

2. Computational Details

2.1. Preparation of Atomic Silica Nanopores. The silica pores used in this work were prepared according to the method proposed by Pellenq and Levitz to prepare numerical Vycor samples.[43] The porous network is carved out of a block of cristobalite (crystalline silica). Then, the pore surface is modeled in a realistic way using the following procedure. We first removed the Si atoms that are in an incomplete tetrahedral environment. We then removed all oxygen atoms that are nonbonded. This procedure ensures that the remaining silicon atoms have no dangling bonds and the remaining oxygen atoms have at least one saturated bond with a Si atom. Then, the electroneutrality of the simulation box was ensured by saturating all oxygen dangling bonds with hydrogen atoms. The latter are placed in the pore void, perpendicular to the pore surface, at a distance of 1 Å from the closest unsaturated oxygen atom. Then, we displace slightly and randomly all the O, Si, and H atoms in order to mimic an amorphous silica surface (the maximum displacement in each direction x, y, and z is 0.7 Å). Full details of the preparation of atomistic silica nanopores can be found elsewhere.[44−46]

The model of silica surfaces used in the present work has been designed to mimic real amorphous surfaces of porous silicas such as Vycor or controlled pore glass. The surface density of OH groups at the pore surface[43] is very close to that obtained experimentally for porous silica glasses (5−7 OH per nm^2).[47,48] On the other hand, the density of OH groups at the surface of MCM-41 is usually smaller (the values reported in the literature range from 2 to 6 OH per nm^2). However, there is a large uncertainty over the experimental materials as far as their surface chemistry is concerned, and the degree of rehydroxylation of the silica surface after synthesis of the sample is usually unknown. In contrast, the simulated materials obtained using the procedure above are able to capture adsorption and condensation of fluids in nanoporous silicas,[43,45,46] and we assume that they provide a reasonable description of real silica polar surfaces which allows us to estimate the effects of confinement and surface chemistry on the stability of confined ZnO nanoparticles. Nevertheless, we acknowledge that significant defects (which are not taken into account in the present work) might affect the local stability of the nanoparticles. Along the same line, morphological pore defects such as pore constrictions or surface roughness might also affect the synthesis of the confined nanoparticles.

The model of MCM-41 considered in this work is a single cylindrical nanopore. Two pore diameters, $D = 1.6$ and 3.2 nm, were considered in order to address the effect of confinement on the stability of ZnO nanostructures. The initial silica matrix is made of $7 \times 7 \times 7$ unit cells of nonporous cristobalite, corresponding to a simulation box of 4.991 nm × 4.991 nm × 4.991 nm. Periodic boundary conditions, which are used to avoid finite size effect, can introduce some artifacts in the case of very small simulation boxes. In order to test the effect of the length of the simulation box we reproduced some of our simulations for the smallest nanopore with a larger simulation cell of 7.843 nm × 7.843 nm × 7.843 nm. Results of these additional simulations are available in the Supporting Information.

2.2. Intermolecular Potentials. ZnO was described in our simulations as ions interacting through interatomic pair potentials. The formal charges +2 and −2 were used for Zn and O, respectively. The interatomic potential energy is the sum of the dispersion (van der Waals) interaction with a short-range repulsive contribution and the Coulombic interactions. We use an analytical expression of the Buckingham type to describe the short-range repulsion and dispersion interactions between two species i and j (Zn or O)

$$U_{ij}(r_{ij}) = A_{ij}\exp(-b_{ij}r_{ij}) - \frac{C_6^{ij}}{r_{ij}^6} \quad (1)$$

where A_{ij}, b_{ij}, and C_6^{ij} are the parameters of the repulsion−dispersion interaction and r_{ij} is the distance between ions i and j. We used a core−shell potential[49] to account for the polarizability of the anion O^{2-}. In the core−shell model the ion consists of a core of charge X and a shell of charge Y such that the total charge is the sum of the core and shell charges (i.e., −2 for O^{2-}). The core and shell are connected by a harmonic spring having a constant k, so that their energy when they are separated by a distance r is

$$U_{CS}(r) = \frac{1}{2}kr^2 \quad (2)$$

The values for the potential parameters A_{ij}, b_{ij}, and C_6^{ij} and the core−shell parameters X, Y, and k were taken from the work by Lewis and Catlow on the calculations of lattice constant, elastic properties, and dielectric constants for ZnO crystals.[50] Table 1 lists the model parameters for the interatomic interactions in ZnO. The electrostatic interactions were calculated using the Ewald summation technique in order to correct the effect of the finite size of the simulation box. The Ewald parameter α was equal to 5.13 Å^{-1}, and the k vectors were such that $|\vec{k}| \leq 7$ (these parameters were chosen according to the criteria proposed by Jackson and Catlow[51]). Reasonable transferability of this interaction potential has been found in the case of the other crystalline phases (as far as some crystalline features or heat capacities are concerned).[52−54] We note that another polarizable model for similar systems has been proposed by Madden and Wilson in their study of covalent effects in ionic liquids or solids.[55−57] In particular, these authors investigated using molecular dynamics simulations the mechanism involved in the wurtzite to rocksalt phase transition.

Interactions between the Zn and O atoms of zinc oxide and the Si, O, and H atoms of the silica nanopore were calculated using the PN-TraZ potential as originally reported for rare gas adsorption in zeolite[58] or porous silica glass.[43] The intermolecular energy is written as the sum of the dispersion interaction with a repulsive short-range contribution, an induction term due to the interaction of the adsorbed atom with the local field created by the partial charges of the atoms in the substrate, and the Coulombic interaction.

Table 1. Parameters for Potential Functions and Core−Shell Model for ZnO (from ref 50)[a]

	A_{ij} (eV)	b_{ij} (Å^{-1})	C_6^{ij}(eV.Å^6)	k (eV Å $^{-2}$)
O_s-O_s	22764.000	6.711	27.880	
$Zn-O_s$	700.30	2.959	0.000	
O_c-O_s				74.92

[a] O_c and O_s denote the core and shell of the anion O^{2-}, respectively. The charges of the core and the shell are $X = 0.86902$e and $Y = -2.86902$e, respectively.

(43) Pellenq, R. J. M.; Levitz, P. E. *Mol. Phys.* **2002**, *100*, 2059.
(44) Coasne, B.; Grosman, A.; Ortega, C.; Pellenq, R. J. M. In *Studies in Surface Science and Catalysis 144*; Rodriguez-Reinoso, F., McEnaney, B., Rouquerol, J., Unger, K., Eds.; Elsevier Science: New York, 2002; p 35.
(45) Coasne, B.; Pellenq, R. J. M. *J. Chem. Phys.* **2004**, *120*, 2913.
(46) Coasne, B.; Pellenq, R. J. M. *J. Chem. Phys.* **2004**, *121*, 3767.
(47) Low, M. J. D.; Ramasubramaniam, N. *J. Phys. Chem.* **1967**, *71*, 730.
(48) Huber, T. E.; Huber, C. A. *J. Phys. Chem.* **1990**, *94*, 2505.
(49) Dick, B. G.; Overhauser, A. W. *Phys. Rev.* **1958**, *112*, 90.
(50) Lewis, G. W.; Catlow, C. R. A. *J. Phys. C* **1985**, *18*, 1149.
(51) Jackson, R. A.; Catlow, C. R. A. *Mol. Sim.* **1988**, *1*, 207.
(52) Zaoui, A.; Sekkal, W. *Phys. Rev. B* **2002**, *66*, 174106.
(53) Sun, X. W.; Chu, Y. D.; Song, T.; Liu, Z. J.; Zhang, L.; Wang, X. G.; Liu, Y. X.; Chen, Q. F. *Solid State Commun.* **2007**, *142*, 15.
(54) Sun, X. W.; Liu, Z. J.; Chen, Q. F.; Yu, J.; Wang, C. W. *J. Phys. Chem. Sol.* **2007**, *68*, 249.
(55) Madden, P. A.; Wilson, M. *Chem. Soc. Rev.* **1996**, *25*, 339.
(56) Madden, P. A.; Wilson, M. *J. Phys.: Condens. Matter* **2000**, *12*, A95.
(57) Madden, P. A.; Wilson, M. *J. Phys.: Condens. Matter* **2002**, *14*, 4629.
(58) Pellenq, R. J. M.; Nicholson, D. *J. Phys. Chem.* **1994**, *98*, 13339.

The choice of the PN-TrAZ model to describe the ZnO/silica interaction was motivated by the good transferability of this model in the case of water in silica glasses[59,60] and benzene in silica nanopores.[61,62] The adsorbate−surface energy $U_k(r_k)$ of the atom k of an adsorbate molecule at a position r_k is given in atomic units by

$$U_k(r_k) = \sum_{j=\{O,Si,H\}} \left[A_{kj} \exp(-b_{kj} r_{kj}) - \sum_{n=3}^{5} f_{2n}(r_{kj}) \frac{C_{2n}^{kj}}{r_{kj}^{2n}} + \frac{q_j q_k}{r_{kj}} \right] - \frac{1}{2} \alpha_k E(r_k)^2 \quad (3)$$

where r_{kj} is the distance between the matrix atom j (O, Si, or H) and atom k of the adsorbate molecule. The first term in eq 3 is a Born−Mayer term corresponding to the short-range repulsive energy due to finite compressibility of electron clouds when approaching the adsorbate to a very short distance from the pore surface. The repulsive parameters A_{kj} and b_{kj} are obtained from mixing rules of like atom pairs (see below). The second term in the above equation is a multipolar expansion series of the dispersion interaction that can be obtained from quantum mechanical perturbation theory applied to intermolecular forces.[63] It has been shown that two-body dispersion C_{2n}^{kj} coefficients for isolated or condensed phase species can be derived from the dipole polarizability and effective number of polarizable electrons N_{eff} of all interacting species[58] which are closely related to the partial charges that can be obtained from ab initio calculations. f_{2n} are damping functions that depend on the distance r_{kj} and repulsive parameter b_{kj}

$$f_{2n}(r_{kj}) = 1 - \sum_{m=0}^{2n} \left[\frac{b_{kj} r_{kj}}{m!} \right] \exp(-b_{kj} r_{kj}) \quad (4)$$

The role of these damping functions is to avoid divergence of the dispersion interaction at a short distance where the wave functions of the two species overlap (i.e., when the interacting species are in contact).[64] For each pair of interacting species they are parametrized with the single b_{kj} repulsive parameter. The third term in eq 3 is the Coulombic interaction between the charge of atom k and that of the substrate atom j. The last term in eq 3 is the induction interaction as written in the context of quantum mechanical perturbation theory applied to intermolecular forces.[63] It represents an attractive energy arising from the coupling of the polarizable electronic cloud of the adsorbate atom of polarizability α_k at position r_k with the electric field $E(r_k)$ induced by the charges carried by the framework species (O, Si, and H). The atomic parameters and coefficients for the ZnO/silica substrate interactions are given in Tables 2 and 3. The repulsive parameters for like pairs are taken from the previous work by Pellenq and Nicholson on the simulation of rare gases in silicalite[58] using the Bohm and Ahlrichs combination rules.[65] This type of potential function based on the PN-TrAZ parametrization method was used in various studies of molecular and covalent fluids at interfaces from open surfaces[59,66] to microporous zeolites[67−71] and more recently in the case of mesoporous silica materials.[43,45,46,59,60,72]

Table 2. PN-TrAZ Potential Parameters for ZnO and Silica Species ($a_0 = 0.529177$ Å and $E_h = 3.1578 \times 10^5$ K)

	zinc oxide		silica		
	Zn	O	Si	O	H
q (e)	+2	−2	+2	−1	+0.5
A_{ij} (E_h)	0.792	836.549	6163.4	1543.5	1.338
b_{ij} (a_0^{-1})	1.004	3.552	2.395	2.19	2.11
α (a_0^3)	8.416	9.980	2.36	8.03	2.25
N_{eff}	8.373	5.656	1.529	4.656	0.324

Table 3. Dispersion and Repulsion Parameters Obtained in the Framework of the PN-TrAZ Model with Bohm and Ahlrichs Combination Rules for Repulsive Interactions

ZnO species	silica species	C_6^{ij} ($E_h \cdot a_0^6$)	C_8^{ij} ($E_h \cdot a_0^8$)	C_{10}^{ij}($E_h \cdot a_0^{10}$)	A_{ij} (E_h)	b_{ij} (a_0^{-1})
Zn	O	43.773	833.019	16234.871	34.957	1.377
Zn	Si	13.271	213.395		69.854	1.415
Zn	H	7.808	109.107		1.029	1.361
O	O	45.506	901.684	18719.081	1136.316	2.709
O	Si	13.743	230.722		2270.680	2.861
O	H	8.498	121.314		33.456	2.647

2.3. Canonical Monte Carlo and Simulated Annealing. The Monte Carlo (MC) technique in the canonical ensemble was used to simulate formation of ZnO nanostructures at 300 K in the atomistic model of MCM-41 silica nanopore. The MC technique in the canonical ensemble is a stochastic method that simulates a system having a constant volume V (the pore with the adsorbed phase), number of particles N, and temperature T.[73−75] Periodic boundary conditions were used along the pore axis so that the system is equivalent to a pore of infinite length. We calculated the adsorbate/substrate interaction using an energy grid;[76] the potential energy is calculated at each corner of each elementary cube (about 1 Å^3). An accurate estimate of the energy is then obtained by a linear interpolation of the grid values. Such a procedure enables simulation of materials confined in nanoporous media of complex morphology and/or topology without a direct summation over matrix species in the course of MC runs.[45,46,77−79]

The ability of MC algorithms to reach equilibrium states in the case of solid structures is often limited by the difficulty of particles to move in dense phases. In order to overcome such metastability barriers, two complementary approaches were adopted in the present work to investigate the stability of the ZnO structures. In the first approach we study the stability of the three crystalline phases of ZnO (wurtzite, rocksalt, and blende) embedded in the silica nanopores. To do so, nanocrystals of each type were cut and inserted in the silica nanopores. After relaxation at 300 K the structure of the confined nanocrystals was studied and compared with those of the ideal ZnO crystals. The second approach adopted in the present work consisted of starting with a homogeneous liquid phase

(59) Puibasset, J.; Pellenq, R. J. M. *J. Chem. Phys.* **2003**, *118*, 5613.
(60) Puibasset, J.; Pellenq, R. J. M. *J. Phys.: Condens. Matter* **2004**, *16*, S5329.
(61) Coasne, B.; Alba-Simionesco, C.; Audonnet, F.; Dosseh, G.; Gubbins, K. E. *Adsorption* **2007**, *12*, 485.
(62) Coasne, B. Alba-Simionesco, C. Audonnet, F. Dosseh, G. Gubbins, K. E., Manuscript in preparation.
(63) Stone, A. *The Theory of Intermolecular Forces*; Oxford and Clarendon: 1996.
(64) Tang, K. T.; Toennies, J. P. *J. Chem. Phys.* **1984**, *80*, 3726.
(65) Bohm, H. J.; Ahlrichs, R. *J. Chem. Phys.* **1982**, *77*, 2028.
(66) Marinelli, F.; Grillet, Y.; Pellenq, R. J. M. *Mol. Phys.* **1999**, *97*, 1207.
(67) Lachet, V.; Boutin, A.; Tavitian, B.; Fuchs, A. H. *J. Phys. Chem. B* **1998**, *102*, 9224.
(68) Nicholson, D.; Pellenq, R. J. M. *Adv. Colloid Interface Sci.* **1998**, *76−77*, 179.
(69) Fuchs, A. H.; Cheetham, A. K. *J. Phys. Chem. B* **2001**, *105*, 7375.
(70) Grey, T. J.; Nicholson, D.; Gale, J. D.; Peterson, B. K. *Appl. Surf. Sci.* **2002**, *196*, 105.
(71) Bichara, C.; Raty, J. Y.; Pellenq, R. J.-M. *Phys. Rev. Lett.* **2002**, *89*, 016101.
(72) Pellenq, R. J. M.; Rousseau, B.; Levitz, P. E. *Phys. Chem. Chem. Phys.* **2001**, *3*, 1207.
(73) Nicholson, D.; Parsonage, N. G. *Computer Simulation and the Statistical Mechanics of Adsorption*; Academic Press: New York, 1982.
(74) Allen, M. P.; Tildesley, D. J. *Computer Simulation of Liquids*; Oxford and Clarendon: 1987.
(75) Frenkel, D.; Smit, B. *Understanding Molecular Simulation: From Algorithms to Applications*, 2nd ed.; Academic Press: London, 2002.
(76) Pellenq, R. J. M.; Nicholson, D. *Langmuir* **1995**, *11*, 1626.
(77) Gelb, L. D.; Gubbins, K. E. *Langmuir* **1998**, *14*, 2097.
(78) Pellenq, R. J. M.; Levitz, P. E. *Mol. Sim.* **2001**, *27*, 353.
(79) Gelb, L. D. *Mol. Phys.* **2002**, *100*, 2049.

confined in the silica pores and cooling the system down to 300 K using Monte Carlo simulations in the canonical ensemble. In order to improve the quality of the sampling in this second set of simulations the MC method was combined with a simulated annealing technique. The latter is a minimization technique that consists of first melting at high temperature the structure to be optimized and then slowly lowering the temperature. Starting with an initial homogeneous structure at high temperature ($T = 4600$ K, which is larger than the melting point of bulk ZnO), the system runs at this temperature for a large number of moves until it reaches equilibrium; each move consists of either randomly selecting and displacing a Zn or a O atom to a new position or randomly displacing the core of a O atom. Then, the temperature is decreased and the system is again allowed to equilibrate; the difference between two successive temperatures is such that $T_{new} = 0.9T_{old}$. The simulation is complete when the temperature reaches the ambient temperature $T = 300$ K. The use of such a high initial temperature enables us to start with a homogeneous liquid of ZnO which is cooled down slowly to obtain well-equilibrated nanostructures within the pores. The silica atoms were maintained fixed in the simulation to avoid melting of the host material. The simulated annealing technique as well as other methods such as the parallel tempering technique do not guarantee reaching full equilibration of the system. However, the simulated annealing technique has proven to be an efficient method to simulate solid phases and materials as it drastically improves the sampling of the phase space compared to regular Monte Carlo or molecular dynamics simulations (as noted by Woodley and Catlow in a very recent review paper, the simulated annealing technique is a very robust technique in predicting crystal structures[80]). By monitoring the evolution of the energy of the confined ZnO nanoparticles in the course of the MC run combined with the simulated annealing technique we checked that the number of MC steps between two successive changes in the temperature is large enough to allow equilibration of the system at each temperature (an example of the evolution of the energy of a confined ZnO nanoparticle in the course of the simulation run is shown in the Supporting Information). We also checked that the nanostructures obtained in the present work are stable when performing additional molecular dynamics molecular simulations. Finally, another indication that the method used in the present work allows reasonable equilibration of the system is as follows. As will be discussed later, when using a larger system size the system was found to converge toward the same nanoparticle morphology ("0D" or "1D") with very similar pair correlation functions and energies per ZnO monomer. Again, although we cannot guarantee that the global minimum has been found, the arguments above suggest that stable states not too far from equilibrium have been reached.

2.4. Molecular Dynamics and Free-Energy Calculations. In order to further characterize the stability of the nanoparticles, we performed additional molecular dynamics simulations at 300 K using the simulation package GULP.[81,82] We also characterized the bulk crystalline ZnO phases (blende, rocksalt, and wurtzite) using molecular dynamics in the canonical ensemble (NVT) in order to obtain reference data to compare our results with. The leapfrog Verlet integration algorithm was used along with the Nose−Hoover thermostat. As for the MC simulations, periodic boundary conditions were used to avoid finite size effects. The same intermolecular potential functions were used as those employed in the MC simulations, and the long-range contribution of the electrostatic interaction was also determined using the Ewald summation technique.

Estimating the free energy of a system is a very difficult task in molecular simulation. In the present work, the free energy of the isolated nanoparticles was determined as follows using the package GULP. Within the harmonic approximation, the internal energy U of the system can be expanded around a local minimum x as

$$U(x+\delta x) = U(x) + \frac{\partial V}{\partial x}\mathrm{d}x + \frac{1}{2!}\frac{\partial^2 V}{\partial x^2}\mathrm{d}x^2 \qquad (5)$$

where $x = \{x_1, x_2, ..., x_i, ..., x_{3N}\}$ is given by the $3N$ coordinates of the N atoms that constitute the system. δx is an infinitesimal variation around the local minimum x. The second and third terms in eq 5 are the first, $g_i = \partial V/\partial x_i$, and second derivatives, $H_{ij} = \partial^2 V/\partial x_i \partial x_j$, of the potential energy V, respectively. H_{ij} constitutes the Hessian matrix of the system, which contains $3N$ rows and $3N$ columns (the Cartesian coordinates of each of the N atoms). Diagonalization of the latter matrix allows estimating the $3N$ normal modes i of vibration of the system as well as their eigenvalue $h\nu_i$. From this phonon spectrum the free energy A_{vib} of the solid system can be estimated by calculating the vibrationnal contribution to its entropy S_{vib} and energy U_{vib}[83,84] within the harmonic approximation (that is valid up to one-half of the fusion temperature).[82] This approach has been used by Shen et al. to estimate the free energy and relative stability of ZnO nanowires and nanotubes as a function of the number of atoms in the periodic unit.[85]

3. Results

3.1. Starting with Ideal Crystal Phases. We first discuss the results obtained using the first approach in which the stability of the three ZnO crystalline phases embedded in the silica nanopores was studied. For the rocksalt and blende structures we orientated the axis (100) of the cubic nanocrystal along the pore axis. In the case of wurtzite the c axis of the nanocrystal was orientated along the pore axis as this crystal axis is known to have the largest growth rate.[86−88] This is due to the fact that the corresponding crystallographic plane (001) is the most reactive surface as it is composed only of O or Zn atoms (i.e., polar surface); in contrast, the other basal crystallographic planes are stoichiometric and therefore less reactive. Taking into account the different growth rates is a difficult and tedious task in molecular simulation that motivated us to complete our study on the stability of the confined ZnO crystalline phases by an approach in which we slowly cool the homogeneous liquid phase down to ambient temperature. We believe that the combination of these two opposite and symmetrical approaches provides interesting insights on the stability of ZnO nanostructures confined in nanopores.

The pair correlation functions $g(r)$ for bulk ZnO crystals at 300 K are shown in Figure 1. Both the Zn−O and Zn−Zn partial contributions are shown. Among these crystals (wurtzite, rocksalt, and blende) wurtzite is the stable phase for ZnO at ambient conditions.[52,89] We also report in Table 4 some properties of these ideal ZnO structures such as the lattice constants (a, c), the equilibrium volumes V_0, and the number and distance of neighbors of like atoms (AA) and unlike atoms (AB). Such numbers and distances can be used to distinguish

(80) Woodley, S. M.; Catlow, R. *Nat. Mater.* **2008**, *7*, 937.
(81) Gale, J. D. *J. Chem. Soc., Faraday Trans.* **1997**, *1*, 629.
(82) Gale, J. D.; Rohl, A. L. *Mol. Simul.* **2003**, *29*, 291.
(83) McQuarrie, D. A. Statistical Mechanics; Harper and Row: New York, 1976.
(84) Hill, T. L. *Statistical Mechanics: Principles and Selected Applications*; Dover Publications: New York, 1987.
(85) Shen, X.; Allen, P. B.; Muckerman, J. T.; Davenport, J. W.; Zheng, J. C. *Nano Lett.* **2007**, *8*, 2267.
(86) Yamabi, S.; Imai, H. *J. Mater. Chem.* **2002**, *12*, 3773.
(87) Wang, X.; Tomita, Y.; Roh, O. H.; Ohsugi, M.; Che, S. B.; Ishitani, Y.; Yoshikawa, A. *Appl. Phys. Lett.* **2005**, *86*, 011921.
(88) Li, G. R.; Dawa, C. R.; Bu, Q.; Zhen, F. L.; Lu, X. H.; Ke, Z. H.; Hong, H. E.; Yao, C. Z.; Liu, P.; Tong, Y. X. *Electrochem. Commun.* **2007**, *9*, 863.
(89) Jaffe, J. E.; Hess, A. C. *Phys. Rev. B.* **1993**, *48*, 7903.

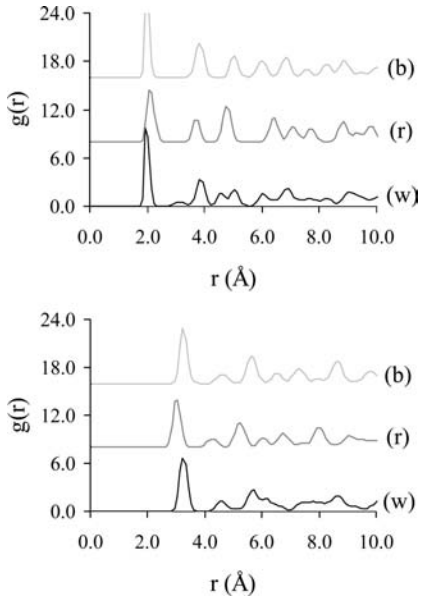

Figure 1. (top) Zn−O pair correlation function $g(r)$ for ideal bulk ZnO crystals: wurtzite (black line), rocksalt (dark gray line), and blende (light gray line). For the sake of clarity, the pair correlation functions for the rocksalt and blende crystals have been shifted by +8 and +16, respectively. (bottom) Same as top for the Zn−Zn pair correlation function $g(r)$.

Table 4. Some Properties for Common Phases of ZnO: Wurtzite (B4), Rocksalt (B1), and Blende (B3)[a]

	wurtzite (B4)	rocksalt (B1)	blende (B3)
V_0 (Å^3)	24.49	19.6	24.65
a (Å)	3.2960	4.28	4.62
c/a	1.580		
$N_{1,\mathrm{AA}}$	12 (3.250)	12 (3.025)	12 (3.275)
$N_{1,\mathrm{AB}}$	4 (2.000)	6 (2.125)	4 (2.025)
$N_{2,\mathrm{AA}}$	6 (4.625)	6 (4.275)	6 (4.625)
$N_{2,\mathrm{AB}}$	1 (3.275)	24 (3.725)	12 (3.825)

[a] Conventional lattice constants (a, c) are related to equilibriulm volumes $V_0 = a^3/4$ (B1, B3) and $V_0 = \sqrt{3}a^2c/4$ (the latter volumes are different from the volumes of the unit cell). $N_{1,\mathrm{AA}}$, $N_{1,\mathrm{AB}}$, $N_{2,\mathrm{AA}}$, and $N_{2,\mathrm{AB}}$ are the number of first and second nearest neighbors of like atoms and unlike atoms, respectively (the number in parentheses is the corresponding distance in Angstroms).

the different crystal phases. Figures 2 and 3 show the pair correlation functions $g(r)$ for the ZnO nanostructures obtained after relaxation at 300 K of the wurtzite, rocksalt, and blende nanocrystals confined in the silica nanopore with $D = 1.6$ and 3.2 nm, respectively. Again, both the Zn−O and Zn−Zn partial contributions are reported for each pore size. None of the nanostructures retains the ideal structure of the initial crystal. The structures obtained from the wurtzite nanocrystal remains crystalline, as marked peaks remain present in the Zn−O and Zn−Zn pair correlation functions. In addition, it can be checked that these peaks belong to the set of peaks observed for the bulk wurtzite crystal (see Figure 1). The structure obtained for the pore with $D = 3.2$ nm exhibits peaks in the $g(r)$ functions that are more marked than those for the small pore. This result is due to the fact that the crystalline structure is less affected by the substrate due to less significant surface constraints in the case of the large pore (the surface to volume ratio of the nanostructure decreases with increasing the pore size). In the case of the pore with $D = 1.6$ nm, both nanostructures obtained from the blende and rocksalt crystals lose their crystalline structures; for both nanostructures the $g(r)$ functions resemble those obtained for liquid or amorphous solids. Even in the case

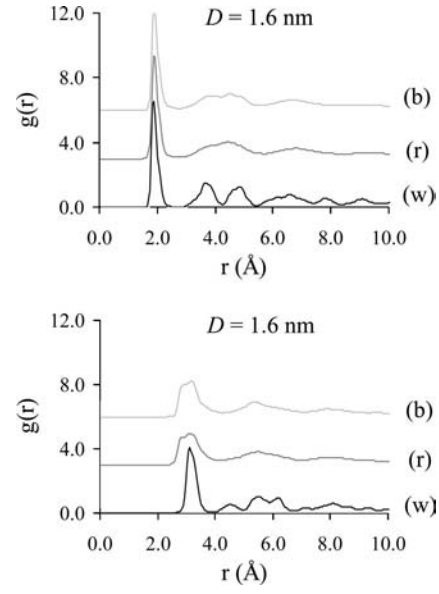

Figure 2. (top) Zn−O pair correlation function $g(r)$ for ZnO crystals confined in a silica nanopore with $D = 1.6$ nm: wurtzite (black line), rocksalt (dark gray line), and blende (light gray line). For the sake of clarity, the pair correlation functions for the rocksalt and blende structures have been shifted by +3 and +6, respectively. (bottom) Same as top for the Zn−Zn pair correlation function $g(r)$.

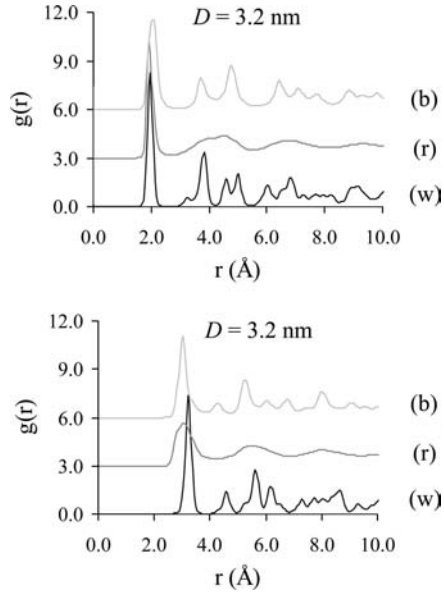

Figure 3. (top) Zn-O pair correlation function $g(r)$ for ZnO crystals confined in a silica nanopore with $D = 3.2$ nm: wurtzite (black line), rocksalt (dark gray line), and blende (light gray line). For the sake of clarity, the pair correlation functions for the rocksalt and blende structures have been shifted by +3 and +6, respectively. (bottom) Same as top for the Zn−Zn pair correlation function $g(r)$.

of the large pore the structure obtained from the rocksalt nanocrystal does not seem to be stable as the $g(r)$ functions obtained for this system after relaxation, which is also characteristic of a noncrystalline structure. On the other hand, the nanostructure obtained from the blende crystal in the pore with $D = 3.2$ nm does possess long-range crystalline order as revealed by the Zn−O and Zn−Zn pair correlation functions $g(r)$ (Figure 3).

We now discuss in detail the local ordering of the nanoparticles obtained above from relaxation of the ZnO crystalline

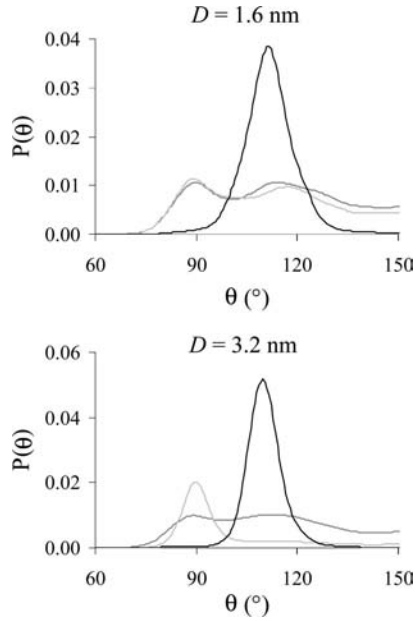

Figure 4. (top) Distribution of angle between Zn−O nearest bonds for ZnO confined in a silica nanopore with $D = 1.6$ nm: wurtzite (black line), rocksalt (dark gray line), and blende (light gray line). (bottom) Same as top for the ZnO confined in a silica nanopore with $D = 3.2$ nm.

phases embedded in the silica nanopores. In particular, we are interested in determining the degree of crystallinity of the particles as well as typical defects. Global crystalline order parameters, which can be used to distinguish bulk crystals as they are sensitive to geometrical and orientational ordering by measuring the coherence of the local bond order,[90,91] are not suitable for confined ZnO nanostructures as the effect of confinement and large degre of disorder of the particles prevent the orientational order of the confined phase from being coherent. Thus, in a first attempt to characterize the confined nanoparticles we followed the work by Ten Wolde et al.,[92] who proposed using local order parameters to distinguish atoms that are crystal-like from atoms that are disordered (liquid or glass-like). Such local order parameters have been found to be suitable to describe freezing in disordered porous materials.[93,94] Unfortunately, the geometrical distortions in the local ordering of the ZnO nanoparticles, which are caused by the small size of the systems and the confinement effect, are too strong and make use of local order parameters not suitable in the present work. In contrast, the $g(r)$ functions as well as the average angle between nearest neighbors were found to be suitable parameters to describe the local ordering of the ZnO confined nanoparticles. Figure 4 shows the angle distribution between Zn−O nearest bonds for the ZnO nanoparticles obtained after relaxation of wurtzite, rocksalt, and blende in the silica nanopore with $D =$ 1.6 nm. We also show in Figure 5 molecular configurations of the nanoparticles. The angle distribution for the nanoparticle obtained from wurtzite exhibits a single peak around ∼110°, which indicates that zinc atoms are mainly ordered according

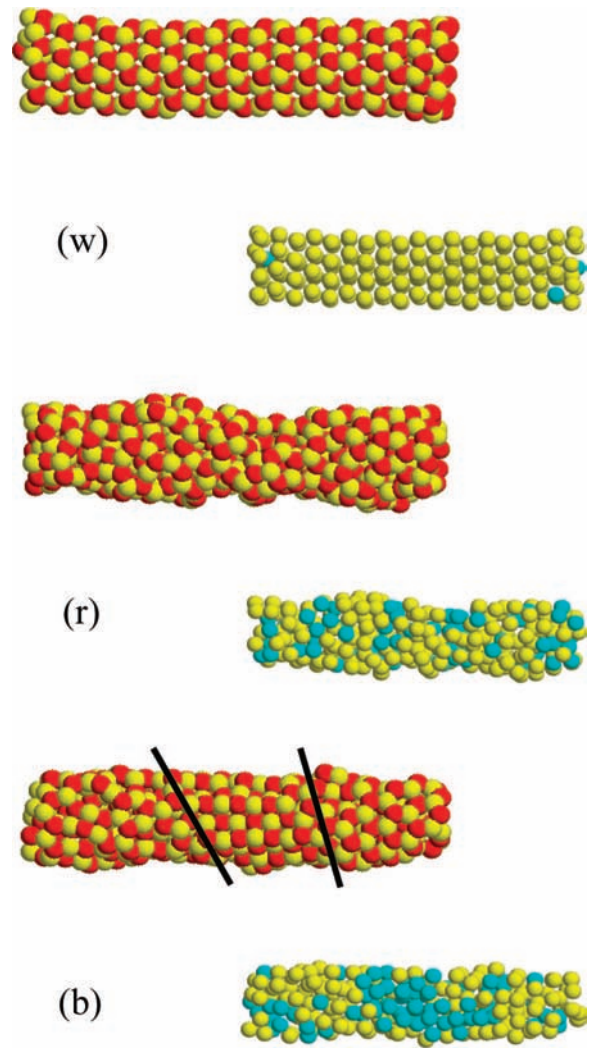

Figure 5. (Color online) Typical molecular configurations of ZnO crystals in a silica nanopore with $D = 1.6$ nm: wurtzite (top), rocksalt (middle), and blende (bottom). The red and yellow spheres are the O and Zn atoms of ZnO, respectively. The two extremities of the pore are connected to each other due to the use of periodic boundary condition along the pore axis. The vertical lines in the bottom-right configuration indicate grain boundaries between wurtzite (left- and right-hand side of the molecular configuration) and blende (middle of the molecular configuration) nanodomains. For each molecular configuration we also show in the right-bottom corner the same image after coloring in yellow zinc atoms that are in a hexagonal-like environment and in cyan zinc atoms that are in a cubic-like environment (see text). The oxygen atoms have been removed for the sake of clarity.

to the hexagonal wurtzite structure. This value is slightly lower than that for bulk wurtzite because the ordering of the atoms at the nanoparticle surface is distorted due to strong constraints. The weak dispersion of the angle distribution for this nanoparticle is consistent with the significant crystal ordering observed in the corresponding pair correlation function (Figure 2). Such a significant ordering also corroborates with the molecular configuration in Figure 5, which shows that the nanostructure obtained from wurtzite keeps the hexagonal structure (triangular symmetry) of the initial nanocrystal. The high degree of triangular symmetry for this nanoparticle is also illustrated in Figure 5 in which we also report the molecular configuration after coloring zinc atoms in a hexagonal-like environment. In contrast to the nanoparticle obtained from wurtzite, those obtained from the rocksalt and blende crystals (Figure 5) exhibit many defects and do not seem to correspond to any known

(90) van Duijneveldt, J. S.; Frenkel, D. *J. Chem. Phys.* **1992**, *96*, 4655.
(91) Lynden-Bell, R. M.; van Duijneveldt, J. S.; Frenkel, D. *Mol. Phys.* **1993**, *80*, 801.
(92) ten Wolde, P. R.; Ruiz-Montero, M. J.; Frenkel, D. *J. Chem. Phys.* **1996**, *104*, 9932.
(93) Coasne, B.; Jain, S. K.; Gubbins, K. E. *Phys. Rev. Lett.* **2006**, *97*, 105702.
(94) Coasne, B.; Jain, S. K.; Naamar, L.; Gubbins, K. E. *Phys. Rev. B* **2007**, *76*, 085416.

crystalline structure (although some local crystalline ordering can be clearly seen). The angle distributions between nearest bonds for these two nanostructures exhibit two peaks around ~87° and 115°, respectively. These values indicate that each of the two nanoparticles are made out of zinc atoms in a hexagonal-like environment and zinc atoms in a cubic-like environment. These two types of zinc environments can be identified in the molecular configurations in Figure 5 where zinc atoms in a hexagonal and cubic packings are distinguished. In particular, two coexisting crystalline domains can be observed for the nanoparticle obtained from the blende crystal, which is a mixture of wurtzite (left and right-hand-side of the molecular configuration) and blende (middle of the molecular configuration) nanodomains. We note that such a coexistence between crystalline domains within nanopores has been already observed in the case of carbon nanotubes casted from $AlPO_4$-5 zeolite.[95]

Figure 4 also shows the angle distribution between Zn−O nearest bonds for the ZnO nanoparticles obtained after relaxation of wurtzite, rocksalt, and blende in the silica nanopore with $D = 3.2$ nm. As in the case of the silica nanopore with $D = 1.6$ nm, the angle distribution for the nanoparticle obtained from wurtzite in the larger pore exhibits a single peak around ~110°. Again, such a value indicates that zinc atoms are mainly ordered according to the hexagonal wurtzite structure. This is supported by the molecular configuration in Figure 6, which shows that the nanostructure obtained from wurtzite keeps the hexagonal structure of the initial nanocrystal (see also in the same figure the molecular configuration in which we distinguish zinc atoms in a local hexagonal environnement). This result also corroborates with the pair correlation in Figure 3, which shows that this nanostructure exhibits significant wurtzite-like crystalline ordering. In contrast, the structure obtained after relaxation of rocksalt in the nanopore with $D = 3.2$ nm exhibits many defects and appears as a disordered nanoparticle with some short-range cyrstalline ordering. The angle distributions between Zn−O nearest bonds for this nanostructure exhibits two peaks around ~87° and 115°, which correspond to zinc atoms in a hexagonal-like and cubic-like environments, respectively. Again, these two types of zinc atoms can be identified in the molecular configurations in Figure 6. Such a distorted nanostructure suggests that even when confined in a large pore of a diameter $D = 3.2$ nm the rocksalt nanocrystal is not stable and evolves toward a structure that exhibits both cubic and hexagonal crystalline orders. More interesting, the angle distribution for the nanoparticle obtained from relaxation of blende in the pore with $D = 3.2$ nm exhibits a single peak around ~90°, which indicates that zinc atoms are mainly ordered according to the cubic structure. This result is consistent with the molecular configuration in Figure 6, which shows that the nanostructure obtained from blende keeps the cubic structure of the initial nanocrystal (although a non-negligible number of zinc atoms in a local hexagonal packing are also found at the particle surface). This result also corroborates with the pair correlation in Figure 3, which shows that this nanostructure exhibits significant blende-like crystal order. This result, which suggests that the blende nanocrystal confined in the nanopore with $D = 3.2$ nm is stable, departs from what was found for the nanopore with $D = 1.6$ nm. In the latter case, the nanostructure obtained after relaxation of the blende nanocrystal was found to be a mixture of wurtzite and blende crystal nanodomains. This result as well as those reported above indicates that the stability of the confined nanocrystals depends in a subtle way on the size of the confining pore.

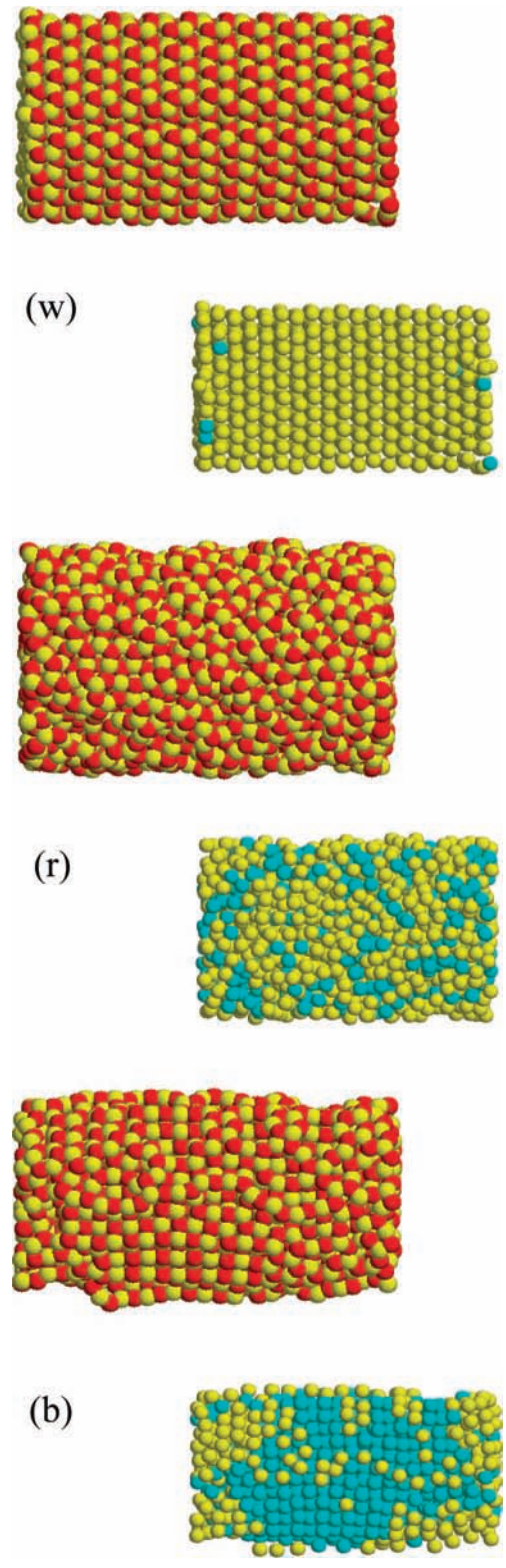

Figure 6. (Color online) Same as Figure 5 but for the silica nanopore with $D = 3.2$ nm.

In order to gain information on the relative stability of the ZnO nanostructures we report in Table 5 the energies (in eV) per ZnO monomer for the ZnO nanostructures obtained atfer relaxation of the wurtzite, rocksalt, and blende crystals in the silica nanopores with $D = 1.6$ and 3.2 nm. For all systems the

(95) Roussel, T.; Pellenq, R. J.-M.; Bichara, C. *Phys. Rev. B* **2007**, *76*, 235418.

Table 5. Energies (eV) per ZnO Monomer for ZnO Wurtzite, Rocksalt, And Blende Confined in Silica Nanopores with $D = 1.6$ and 3.2 nm[a]

	wurtzite (B4)		rocksalt (B1)		blende (B3)	
	$D = 1.6$ nm (228)	$D = 3.2$ nm (1311)	$D = 1.6$ nm (243)	$D = 3.2$ nm (1575)	$D = 1.6$ nm (219)	$D = 3.2$ nm (1191)
confined						
E	−500.8	−96.6	−472.2	−86.8	−519.7	−102.2
$E_{ZnO/ZnO}$	−39.0	−39.4	−38.8	−39.0	−38.8	−39.2
$E_{ZnO/silica}$	−461.8	−57.3	−433.5	−47.7	−480.8	−63.0
F	−39.0		−38.9		−38.9	
free						
$E_{ZnO/ZnO}$	−39.1	−39.4	−38.9	−39.1	−38.9	−39.2

[a] The number in parentheses indicates the number of ZnO monomers for each nanostructure. For all systems the total energy E as well as the ZnO−ZnO and ZnO−Silica contributions are shown. We also report the free energy F of the nanoparticle which has been determined from the Hessian matrix (see text). The energy of the "free" nanostructure which has been relaxed after removal of the host silica matrix is shown in the last line of the table.

total energy E as well as the ZnO−ZnO and ZnO−silica contributions are presented. We also report in Table 5 the free energy of the nanoparticle, which has been obtained using the Hessian matrix as described in section 2. Given the size of the Hessian matrix to be diagonalized, it is not feasible to determine the free energy of large systems and only the free energy of nanoparticles confined in the silica nanopore of diameter $D = 1.6$ nm are shown (these results are, however, the most interesting as we expect largest effects for the small nanoparticles, i.e., particles having a large surface to volume ratio). For a given pore size the ZnO−ZnO contribution ($E_{ZnO/ZnO}$) to the total energy of the structures obtained from the relaxation of the wurtzite, rocksalt, and blende crystals are such that $E_W < E_B \approx E_R$. This inequality suggests that the structure obtained from the wurtzite crystal is the most stable structure followed by that obtained from the blende crystal. This relative stability between the different phases is not changed when one looks at the free energy of the nanoparticle instead of the energy. This is due to the fact that the vibrational contribution (entropy + energy) to the total free energy is small, ∼0.04−0.1 eV/ZnO monomer, compared to the total energy. We note that the values reported above for the energy and free energy of the nanoparticles are consistent with what is usually found for solid phases; the energy is of the order of magnitude of kJ/mol, while the entropy is of the order of magnitude of J/mol. These values are also consistent with the work by Shen et al.,[85] who found that the free energy lowering ($T\Delta S$) between a ZnO nanotube and nanowire composed of the same number of atoms is about 10 k_BT (∼0.02 eV/ZnO monomer). For each initial crystalline structure the typical value of $E_{ZnO/ZnO}$ for the nanopore with $D = 1.6$ nm is larger (less attractive) by 0.2−0.4 eV than that for the nanopore with $D = 3.2$ nm. This result reflects that the surface to volume ratio decreases when the pore size increases. For very large pore sizes one should recover the typical value of the ZnO−ZnO interaction in crystal phases, ∼39.5−39.7 eV (see Figure 5 in ref 52). The effect of surface to volume ratio can also be seen in the ZnO−silica contribution to the total energy (per pair of ZnO atoms), which is about 7−9 times larger for the small pore than for the large pore.

We also report in Table 5 the energy of the 'free' nanostructures after removal of the host silica matrix. These energies correspond to the energy after relaxation at 300 K of the free nanostructures. Due to the relaxation in which the initial stresses caused by the porous silica matrix are released, the energy of the nanostructure after removal of the host material is lower (more attractive) than that of the embedded nanostructure. The decrease in the energy per pair of ZnO is about 0.1 eV (whatever the initial crystalline structure wurtzite, rocksalt, or blende). Such a low gain in the stability of the nanostructure suggests that the 'free'nanostructure remains close to the embedded structure. This result also corroborates with the Zn−O pair correlation functions $g(r)$ (not shown) for the free structures, which were first obtained from the rocksalt and wurtzite crystals in the silica nanopore with $D = 1.6$ nm. The latter show that the pair correlation functions for the nanostructures relaxed before and after removal of the host material are almost identical.

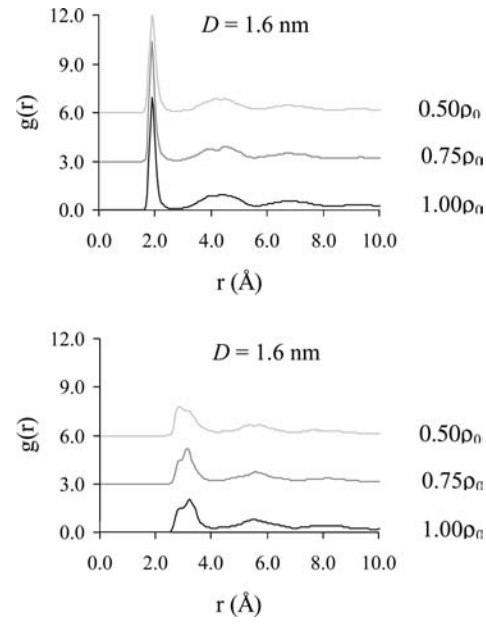

Figure 7. (top) Zn−O pair correlation function $g(r)$ for ZnO confined in a silica pore with $D = 1.6$ nm for three different densities: (from bottom to top) $\rho = \rho_0$, $\rho = 0.75\rho_0$, and $\rho = 0.50\rho_0$. For the sake of clarity, the pair correlation function for the densities $\rho = 0.75\rho_0$ and $\rho = 0.50\rho_0$ have been shifted by +3 and +6, respectively. (bottom) Same as top for the Zn−Zn pair correlation function $g(r)$.

3.2. Starting with Liquid Phases. We now discuss the results obtained using our second approach, which consists of starting with a homogeneous liquid phase confined in the silica pores with $D = 1.6$ and 3.2 nm and cooling the system down to 300 K. In this part of the work we also investigated for both nanopores the effect of the filling density of the porosity. To do so, we filled the porosity with three densities $\rho = 0.50\rho_0$, $0.75\rho_0$, and $1.00\rho_0$, where ρ_0 is the density of particles in the bulk ZnO wurtzite crystal. A filling density ρ means that the total pore volume V is filled with a number of atoms $N = \rho V$. Investigation of the effect of the filling density on the structure and morphology of confined ZnO nanoparticles has been motivated by the experiments by Polarz et al.,[34] who found that most samples contain nanoparticles that are much smaller than the pore size, i.e., even if the pore is entirely filled by the liquid reactants, the synthesized ZnO nanoparticles do not fully occupy the porous space. The results below were obtained with a simulation box of a length 4.991 nm. However, we tested the effect of the length of the simulation box by reproducing our simulations for the smallest nanopore $D = 1.6$ nm with a larger simulation cell of a length 7.843 nm. Results of these additional simulations are available in the Supporting Information.

Figure 7 shows the pair correlation functions $g(r)$ for the ZnO nanostructures obtained after relaxation for the three densities

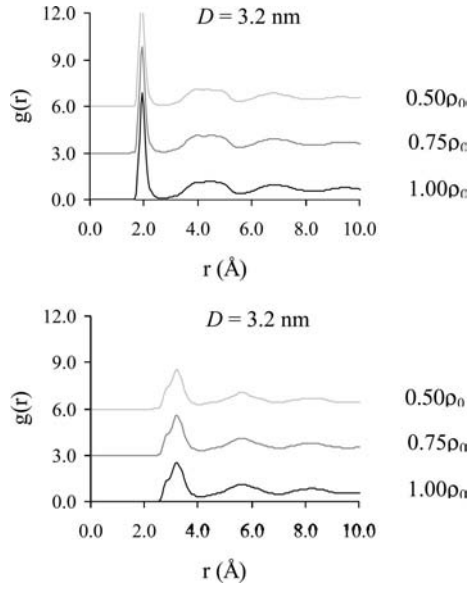

Figure 8. (top) Zn−O pair correlation function $g(r)$ for ZnO confined in a silica pore with $D = 3.2$ nm for three different densities: (from bottom to top) $\rho = \rho_0$, $\rho = 0.75\rho_0$, and $\rho = 0.50\rho_0$. For the sake of clarity, the pair correlation function for the densities $\rho = 0.75\rho_0$ and $\rho = 0.50\rho_0$ have been shifted by +3 and +6, respectively. (bottom) Same as top for the Zn-Zn pair correlation function $g(r)$.

in the silica nanopore with $D = 1.6$ nm. Both the Zn−O and Zn−Zn partial contributions are reported for each density. We report the same curves in Figure 8 for the ZnO nanostructures obtained for the pore with $D = 3.2$ nm. For all filling densities the structure obtained after cooling the system to 300 K does not exhibit crystalline features, although some significant correlations are observed for the first and second nearest neighbors: (1) the first peak in the Zn−O $g(r)$ function has a large amplitude (∼6.8) compared to what is usually observed for molecular liquids, (2) the second peak in the Zn−O $g(r)$ function is split into two secondary peaks, and (3) the first peak in the Zn−Zn $g(r)$ function presents a shoulder on its left. Such a local ordering of the ZnO nanostructure within the pore seems independent of the pore filling as the pair correlation functions for the three densities are very similar. In addition, the pore size does not seem to affect significantly the structure of the ZnO nanomaterial as the pair correlation functions for the pore with $D = 1.6$ nm resemble those for the pore with $D = 3.2$ nm. From these pair correlation functions we estimated the number of first nearest neighbors of like atoms ($N_{1,AA}$) and unlike atoms ($N_{1,AB}$) using the following relation

$$N_{i,AB} = 4\pi\rho\int_i r^2 g_{AB}(r)\mathrm{d}r \qquad (6)$$

where $N_{i,AB}$ denotes the number of ith nearest neighbors of atoms A and B (A, B = Zn or O). The integration in eq 6 runs over the range of distances r corresponding to the ith neighbor. The density ρ is taken as ρ_0, i.e., the density of particles in the bulk ZnO wurtzite crystal. Although the density of pore filling is not constant in our simulations, we used for all calculations of nearest neighbors $\rho = \rho_0$ as the density of the nanostructure obtained after relaxation is found to be close to that of the bulk material. In fact, the density of the nanostructure ($\sim\rho_0$) differs from the filling density ($\leq\rho_0$), which is an apparent density of ZnO within the nanopore. In the case of the filling density $\rho = \rho_0$ we found $N_{1,AA} = 10.1$ and $N_{1,AB} = 3.8$ for the pore with $D = 3.2$ nm and $N_{1,AA} = 8.3$ and $N_{1,AB} = 3.5$ for the pore with $D = 1.6$ nm. For a given pore size similar values were found for the other filling densities. Such numbers of nearest neighbors of like and unlike atoms are close to those for the ideal bulk wurtzite and blende crystals, i.e., $N_{1,AA} = 12.0$ and $N_{1,AB} = 4.0$ (see Table 4). In addition, the location of the peaks corresponding to the distances between nearest neighbors of like and unlike atoms ($d_{1,AA} = 3.275$ Å and $d_{1,AB} = 1.975$ Å) are very close to those of the bulk wurtzite and blende structures. These results suggest that the stable phase (starting from the homogeneous liquid phase) is closer to one of these ideal structures than to the rocksalt structure. This result is consistent with those reported above, showing that the confined rocksalt structure does not remain stable when relaxed at 300 K. The fact that the number of nearest neighbors $N_{1,AA}$ and $N_{1,AB}$ are smaller than those for the bulk structures is due to the atoms located at the interface between the nanostructure and the silica surface which possess a smaller coordination number. This result also corroborates with the fact that these numbers are smaller for the pore with $D = 1.6$ nm than for the pore with $D = 3.2$ nm (as the ratio of surface atoms to volume atoms increases with decreasing the pore size).

Figures 9 and 10 show typical molecular configurations of the ZnO nanostructures obtained atfer cooling to 300 K the homogeneous liquids ($\rho = 0.50\rho_0$, $\rho = 0.75\rho_0$, and $\rho = 1.00\rho_0$) in the silica nanopores with $D = 1.6$ and 3.2 nm, respectively. In the case of the pore with $D = 3.2$ nm we found that ZnO forms nanorods (quasi-1D systems) for all filling densities. However, the nanostructure exhibits dispersion in its diameter along its axis as the filling density decreases. Interestingly, the nanostructures obtained for $\rho = 0.50\rho_0$ and $0.75\rho_0$ are faceted, as is usually observed for larger bulk-like crystals. This result suggests that the size of these nanoparticles is large enough to recover a 3D-like behavior. The origin of such crystalline faces differs from the octaedral shape of the particle obtained for $\rho = \rho_0$, which is imposed by the morphology of the silica host nanopore. In contrast to these results for the large pore, the morphology of the nanostructure in the case of the pore with $D = 1.6$ nm depends on the filling density of the porosity. ZnO arranges itself to form nanorods (quasi-1D systems) for $\rho = 0.75\rho_0$ and ρ_0, while a nanoparticle (dimensionality "0D") is observed for $\rho = 0.50\rho_0$. In the latter case, the nanostructure is composed of (1) a nanoparticle that spreads over the diameter of the nanopore and (2) a chain of ZnO atoms that connects the nanoparticle through the left and right sides of the simulation box (which are physically connected due to the use of periodic boundary conditions). Such defects are similar to those observed by Wilson in his study of KI confined in carbon nanotubes.[41] It must be emphasized that such a strictly 1D chain of ZnO atoms, which is stable over the length of the simulation run, is probably metastable and would probably disappear to merge with the larger nanoparticle if longer simulation runs were performed. This result is supported by our preliminary work in which we reported formation of an isolated nanoparticle within a silica nanopore.[96] We note that for the filling density $\rho = 0.5\rho_0$ the cross-section for the nanopore with $D = 1.6$ nm suggests that the pore is "more filled" than the pore with $D = 3.2$ nm (for which the cross-section shows that there is some unfilled porous space in the cross-section). This is due to the fact that the nanostructure is an isolated nanoparticle for the pore with $D = 1.6$ nm instead of a nanorod for the pore with $D = 3.2$ nm. On one hand, for the nanopore with $D = 1.6$ nm ZnO fills only

(96) Mezy, A.; Suwanboon, S.; Ravot, D.; Coasne, B.; Tedenac, J. C.; Bretagnon, T.; Lefebvre, P.; Gerardin, C.; Pichon, B.; Tichit, D. *Proceedings of the Conference "Materiaux 2006"*, Dijon, France, 2006.

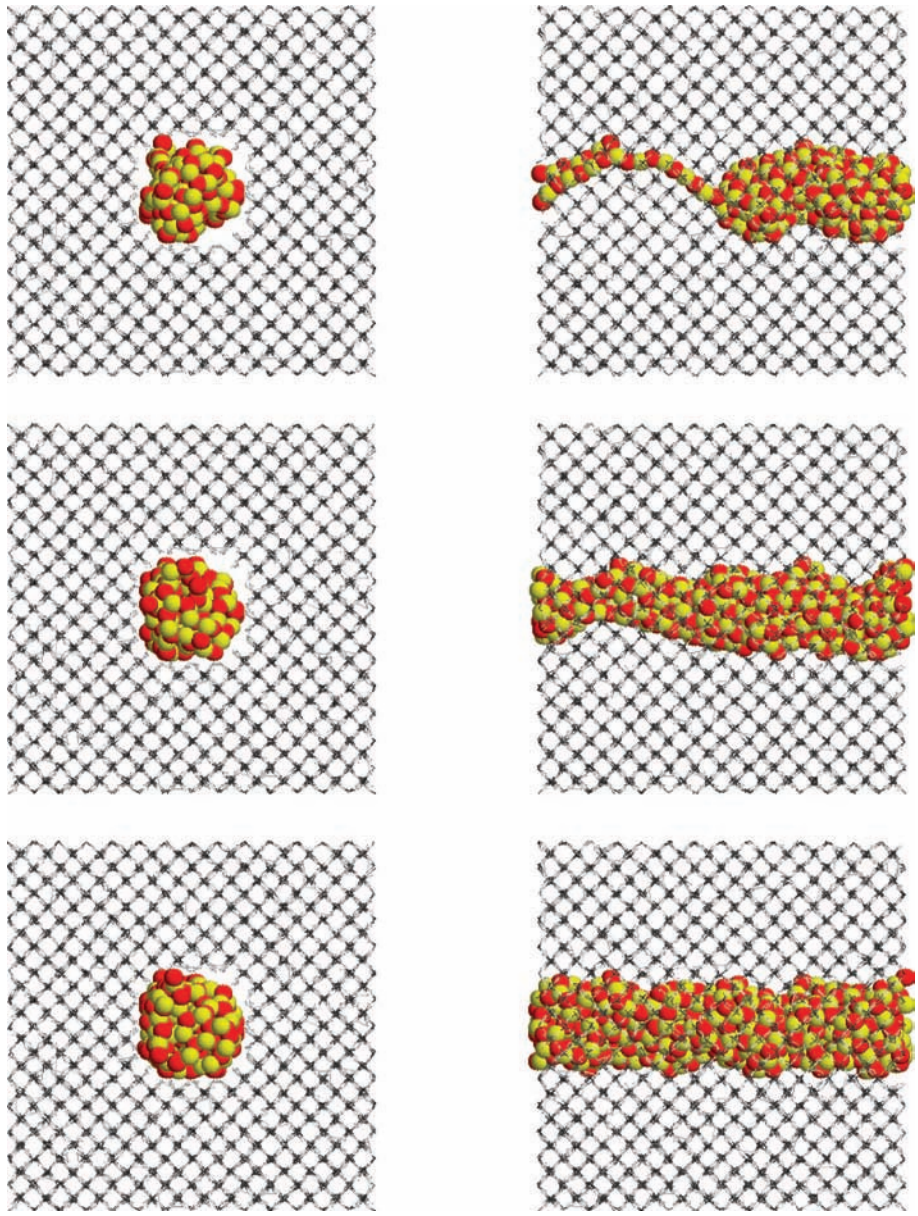

Figure 9. (Color online) Cross-section (left) and transverse (right) views of typical molecular configurations of ZnO confined in a silica nanopore with $D = 1.6$ nm for three densities: (from bottom to top) $\rho = \rho_0$, $0.75\rho_0$, and $0.50\rho_0$. The red and yellow spheres are the O and Zn atoms of ZnO, respectively. The small white and dark gray spheres connected by segments are the O and Si atoms of the silica nanopore (the H atoms at the pore surface of the host material are not shown for the sake of clarity).

one-half of the porous space along the pore axis but spreads over the entire cross-section. On the other, for the nanopore with $D = 3.2$ nm ZnO fills only one-half of the cross-section of the pore but spreads over the entire pore length. As a result, although the two pores are filled with the same filling density, the cross-section for the nanopore with $D = 1.6$ nm gives the misleading visual impression that the pore is fully filled as the cross-section of the pore seems to be entirely obstructed by the ZnO nanoparticle.

Another important finding of the present work concerns the surface polarity of the resulting nanostructures. Density profiles (not shown) show that all of the nanoparticles in this work exhibit neutral (basal) faces, i.e., faces terminated with both Zn and O atoms in the same stoichiometry (in contrast to polar surfaces terminated by a plane composed entirely of atoms of the same species). This is due to the symmetry of the cylindrical nanopore that imposes that the Zn and O atoms must be distributed equally along the radial direction. This prevents the system from having surfaces of different polarities (the same argument also holds for a slit pore).

Table 6 reports the energies (in eV) per ZnO monomers for the ZnO nanostructures obtained after cooling to 300 K the homogeneous liquids ($\rho = 0.50\rho_0$, $0.75\rho_0$, and $1.00\rho_0$) in the silica nanopores with $D = 1.6$ and 3.2 nm. For all systems, the total energy E as well as the ZnO−ZnO ($E_{\mathrm{ZnO/ZnO}}$) and ZnO−silica ($E_{\mathrm{ZnO/silica}}$) contributions are presented. We also report in Table 6 the free energy of the nanoparticle which has been obtained from the Hessian matrix as described in section 2. Again, due to the size of the Hessian matrix to be minimized we show only the results of our free energy calculations for confined nanoparticles with less than ~900 ZnO monomers (see the discussion above). Independent of the pore size, $E_{\mathrm{ZnO/ZnO}}$ decreases (becomes more attractive) as the number of pairs of ZnO increases. In contrast, $E_{\mathrm{ZnO/silica}}$ increases (becomes less

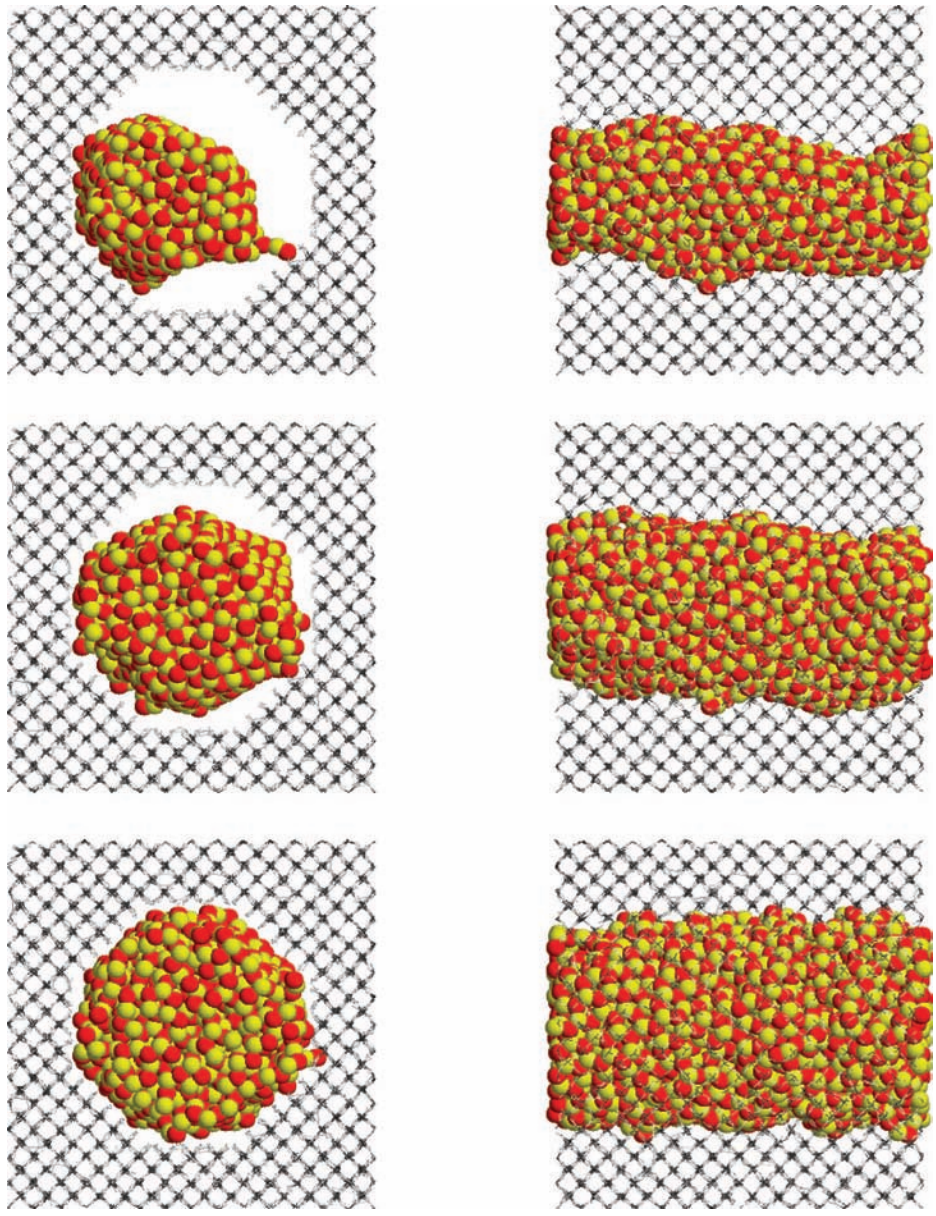

Figure 10. (Color online) Cross-section (left) and transverse (right) views of typical molecular configurations of ZnO confined in a silica nanopore with $D = 3.2$ nm for three densities: (from bottom to top) $\rho = \rho_0$, $0.75\rho_0$, and $0.50\rho_0$. The red and yellow spheres are the O and Zn atoms of ZnO, respectively. The small white and dark gray spheres connected by segments are the O and Si atoms of the silica nanopore (the H atoms at the pore surface of the host material are not shown for the sake of clarity).

attractive) with increasing the number of ZnO monomers. Again, these results reflect that the surface to volume ratio decreases when the pore size increases or when the number of ZnO monomers increases. In the case of the pore with $D = 3.2$ nm, $E_{ZnO/ZnO}$ is constant about at -39.1 eV for all densities. This result suggests that the bulk-like behavior is recovered for these particles containing more than 600 monomers, in agreement with our previous conclusion on the observation of faceted nanoparticles. This result is also supported by the fact that the typical value for $E_{ZnO/ZnO}$ is close to those for ideal crystal phases, 39.5−39.7 eV (see ref 52). As observed above for the nanocrystals confined in the silica nanopores, the vibrational contribution (entropy + energy) is found to be small, ∼0.04−0.1 eV/ZnO monomer, compared to the total free energy. These values suggest that this contribution is not the key parameter in determining the relative stability of the different particles (the energy is on the order of magnitude of kJ/mol, while the entropy is on the order of magnitude of J/mol as expected for solid phases).

We also report in Table 6 and Figure 11 the energy of the 'free' nanostructures after removal of the host silica matrix. These energies correspond to the energy after relaxation of the nanostructure. Again, due to the relaxation in which the initial stresses caused by the porous silica matrix are released, the energy of the nanostructure after removal of the host material is lower (more attractive) than that of the embedded nanostructure. The decrease in the energy per pair of ZnO is about 0.1−0.2 eV for the small pore (large surface to volume ratio) and 0.05 eV for the large pore (small surface to volume ratio).

4. Discussion

This paper reports a molecular simulation study of ZnO nanostructures confined within cylindrical silica nanopores of

Table 6. Energies (eV) per ZnO Monomer for Nanostructures Obtained in Silica Nanopores with $D = 1.6$ and 3.2 nm Filled with Three Densities $\rho = 0.50\rho_0$, $0.75\rho_0$, and ρ_0[a]

	$D = 1.6$ nm			$D = 3.2$ nm		
	$0.50\rho_0$ (108)	$0.75\rho_0$ (161)	ρ_0 (215)	$0.5\ \rho_0$ (610)	$0.75\rho_0$ (915)	ρ_0 (1220)
confined						
E	−1013.7	−692.9	−528.8	−162.1	−121.1	−100.7
$E_{ZnO/ZnO}$	−38.6	−38.7	−38.8	−39.1	−39.1	−39.1
$E_{ZnO/Silica}$	−975.2	−654.2	−490.0	−123.0	−82.0	−61.6
F	−38.7	−38.8	−38.9	−39.0		
free						
$E_{ZnO/ZnO}$	−38.8	−38.9	−38.9	−39.1	−39.1	−39.1

[a] The number in parentheses indicates the number of ZnO monomers for each nanostructure. For all systems the total energy E as well as the ZnO−ZnO and ZnO−Silica contributions are shown. We also report the free energy F of the nanoparticle which has been determined from the Hessian matrix (see text). The energy of the "free" nanostructure which has been relaxed after removal of the host silica matrix is shown in the last line of the table.

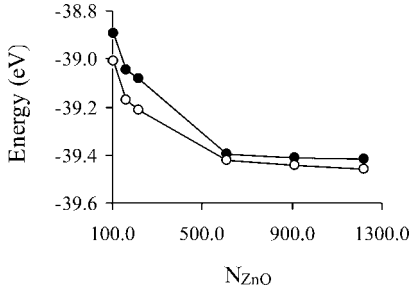

Figure 11. Energy per ZnO monomer as a function of the number of monomers ZnO for nanostructures obtained in silica nanopores with $D = 1.6$ and 3.2 nm filled with three densities $\rho = \rho_0$, $0.75\rho_0$, and $0.50\rho_0$. For all systems the energy corresponds to the ZnO−ZnO contribution per ZnO monomer. The black symbols correspond to the energy when the nanostructure is embedded in the pore. The white symbols correspond to the energy of the nanostructure which has been relaxed after removal of the host silica matrix.

diameter $D = 1.6$ and 3.2 nm. The simulations of the ZnO nanomaterial embedded in the porous matrix are carried out using the Monte Carlo algorithm in the canonical ensemble. Both the effect of confinement (by varying the pore size) and that of the degree of pore filling on the structure of the nanomaterial are addressed. The pores used in this work are carved out of an atomistic block of silica in order to obtain fully atomistic nanopores (then the pore surface is modeled in a realistic way by saturating the oxygen dangling bonds at the pore surface by hydrogen atoms). In order to overcome metastability barriers in formation of dense nanostructures, two complementary approaches are adopted in the present work. We first study the stability of the three crystalline phases of ZnO (wurtzite, rocksalt, and blende) embedded in the silica nanopores. To do so, nanocrystals of each type are cut and inserted in the silica nanopores and then relaxed at 300 K. The second approach consists of starting with a homogeneous liquid phase confined in the silica pores and cooling the system to 300 K using Monte Carlo simulations combined with a simulated annealing technique.

None of the ideal nanostructures (wurtzite, rocksalt, blende) retains the ideal structure of the initial crystal when confined and relaxed within the silica pores. Only the structure obtained from the wurtzite nanocrystal remains crystalline, as revealed by the marked peaks in the pair correlation functions for this system. In the case of the pore with $D = 3.2$ nm the peaks in the $g(r)$ functions are more marked than those for the small pore. This result is due to the fact that the crystalline structure is less affected by the substrate due to less significant surface constraints in the case of the large pore. In the case of the pore with $D = 1.6$ nm both the nanostructures obtained from the blende and rocksalt crystals seem to lose their crystalline structures; for both nanostructures the $g(r)$ functions resemble those obtained for liquid or amorphous solids. Even in the case of the large pore the structure obtained from the rocksalt nanocrystal does not seem to be stable as the $g(r)$ functions obtained for this system after relaxation are also characteristic of a noncrystalline structure. For a given pore size the ZnO−ZnO contribution to the energy ($E_{ZnO/ZnO}$) of the structures obtained from the relaxation of the wurtzite, rocksalt, and blende crystals are such that $E_W < E_B \approx E_R$. This inequality suggests that the structure obtained from the wurtzite crystal is the most stable structure followed by that obtained from the blende crystal. This result is consistent with the typical molecular configurations of these systems; the nanostructure obtained from the wurtzite crystal keeps the hexagonal structure (triangular symmetry) of the initial material, while that obtained from the rocksalt crystal exhibits many defects and does not seem to correspond to any obvious crystalline structure. Finally, the structure obtained from the blende crystal presents an interesting structure which is a mixture of wurtzite and blende nanodomains.

In this paper, we also considered the case of confined nanostructures obtained by cooling down to 300 K a homogeneous liquid phase. In this case, the effect of the filling density of the pore was also investigated for both the nanopores with $D = 1.6$ and 3.2 nm. Starting with the homogeneous liquid phase we found that the structure obtained after cooling does not exhibit clear crystalline features, although some significant local ordering is observed. Our results suggest that the pore size does not affect the structure of the ZnO nanomaterial as the pair correlation functions for the pore with $D = 1.6$ nm is very close to those for the pore with $D = 3.2$ nm. In addition, based on the number and distances of first nearest neighbors of like and unlike atoms we found that the local ordering of the confined nanostructures is close to that for ideal bulk wurtzite and blende crystals. This result is consistent with those obtained when starting with ideal crystal phases, which show that the confined rocksalt structure does not remain stable when relaxed at 300 K. An interesting result of the present study is that the morphology and dimensionality of the nanostructure depends on the filling density of the silica pore with ZnO monomers. In the case of the large pore we found that ZnO forms nanorods (dimensionality 1D) for all filling densities and the nanostructures are faceted, which suggests that the size of the nanoparticles is large enough to recover a bulk-like behavior. In contrast, the morphology of the nanostructure in the case of the smaller pore depends on the filling density of the porosity. ZnO arranges itself either as nanorods for large filling densitites or as an isolated nanoparticle for low filling density. Another finding is that the use of confining materials (such as cylindrical or slit-shaped pores) imposes that the nanoparticles exhibit basal surfaces only.

Our results show that, independent of the pore size, the ZnO−ZnO contribution to the total energy ($E_{ZnO/ZnO}$) becomes more attractive as the number of pairs of ZnO increases. In contrast, the ZnO−silica contribution ($E_{ZnO/silica}$) becomes less attractive with increasing number of ZnO monomers. These results reflect the decrease in the surface to volume ratio of the nanoparticles as the pore size increases. In the case of the large

pore ($D = 3.2$ nm), $E_{ZnO/ZnO}$ is constant at about -39.1 eV for all filling densities, which suggests that the bulk-like behavior is recovered for these particles containing more than 600 monomers ($E_{ZnO/ZnO}$ for ideal crystal phases is about $39.5-39.7$ eV). For all systems studied in this work the nanostructures embedded in the nanopores were relaxed after removal of the host silica matrix. Due to the relaxation that suppresses the stresses caused by the porous silica material, the energy of the nanostructure after removal of the host material is lower (more attractive) than that of the embedded nanostructure (for all systems the decrease in the energy per pair of ZnO remains small as the decrease in the energy per pair of ZnO atoms is at most $0.1-0.2$ eV).

5. Conclusion and Future Work

None of the nanoparticles otbained in the present work exhibit clear crystalline features, although some significant local geometrical ordering is observed. Even nanoparticles obtained after relaxation of ideal nanocrystals (wurtzite, blende, rocksalt) exhibit significant defects. This result is in agreement with the work of Jentys and Grimes,[35] who performed atomistic simulations of ZnO in siliceous zeolites and observed significant geometrical disortions of the confined clusters. The results obtained in the present work are also in agreement with the experimental work by Polarz et al.,[34] who studied ZnO nanoclusters confined in the pores of a host silica porous material by means of X-ray diffraction and EXAFS. In agreement with our results on the effect of pore size on the structure of confined ZnO nanoparticles, these authors showed that the degree of crystallinity of the synthesized nanostructure decreases as the pore size decreases (see Figure 7 in ref 34). Polarz et al. also found that ZnO nanoparticles obtained for a nanopore of a diameter of $D = 1.8$ nm are nearly amorphous and exhibit much less long-range crystalline order,[34] in agreement with our results for a pore of a diameter $D = 1.6$ nm.

In this work we also found that that confined relaxed nanocrystals (wurtzite, blende, rocksalt) have different relative stabilities. In particular, in the case of the smallest nanopore we were able to observe a particle which is composed of a mixture of wurtzite and blende nanodomains. This result is consistent with the experimental work by Seo et al.[19] These authors showed by means of field-emission scanning electron microscopy and X-ray diffraction that ZnO nanoparticles obtained within the channels of porous alumina have polycrystalline structural properties. The observation of different possible crystalline phases is also consistent with the work of Kulkarni et al.,[36,37] who found that crystalline phase transitions in ZnO nanowires occur under uniaxial tensile loading. In the case of confined nanoparticles such as those in the present work, the non-negligible interaction with the pore surface introduces an anisotropic constraint on the nanostructure, which may trigger transformations similar to those reported by Kulkarni et al. Finally, shifts in the relative stability of crystalline phases upon confinement is also in agreement with experiments[39] and molecular simulations[41] on confined salts showing that freezing occurs at a temperature different from the bulk and that phase stability is affected by confinement. Depending on the filling density of the pores we also observed different particle morphologies such as an isolated nanoparticle or nanowires. In contrast, no hollow particle such as ZnO nanotube has been observed. This result is consistent with the work by Shen et al.,[85] who investigated the stability of small one-dimensional ZnO nanostructures using ab initio calculations. These authors found that the nanorod (filled particle) has a lower energy (more stable) than the nanotube (hollow particle) when it is composed of a number of atoms larger than 38 (the smallest ZnO particle in the present work has 216 atoms).

In future work, we plan to extend the present work as follows. The pair potentials we used were developed to reproduce the structural properties of ZnO wurtzite. Although reasonable transferability of this interaction potential has been found in the case of the other crystalline phases (as far as some crystalline features or heat capacities are concerned),[52−54] care must be taken when discussing the relative stability of the different ZnO nanocrystals. In order to gain information independent of the validity of the potential used to describe the interactions between the Zn and O atoms, we plan to study in future work the stability of the ZnO nanostructures confined in the same atomistic models of silica pores using other potentials. For this purpose we note that another polarizable model for ionic systems has been proposed by Madden and Wilson.[55,56] Finally, more ZnO realistic potentials have been also proposed in the literature, including a bond-order potential[97] and a tight-binding potential.[98] We also envisage performing first-principles calculations on the ZnO nanostructures obtained in the present work in order to estimate their electronic and optical properties. Finally, other porous materials (such as carbon nanotubes) can be also considered to vary the nature of the host matrix and determine the role of the surface chemistry in formation of confined nanostructures.

Supporting Information Available: Additional simulation results obtained using a larger simulation box. This material is available free of charge via the Internet at http://pubs.acs.org.

JA806666N

(97) Erhart, P.; Juslin, N.; Goy, O.; Nordlund, K.; Muller, R.; Albe, K. *J. Phys.: Condens. Matter* **2006**, *18*, 6585.
(98) Fang, T. H.; Chang, W. J.; Chiu, J. W. *Microelectron. J.* **2006**, *37*, 722.